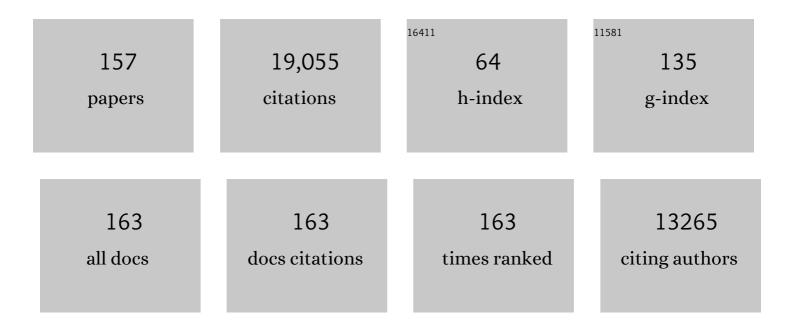
## Sebastien Boutet

List of Publications by Year in descending order

Source: https://exaly.com/author-pdf/9061589/publications.pdf Version: 2024-02-01



#	Article	IF	CITATIONS
1	Femtosecond X-ray protein nanocrystallography. Nature, 2011, 470, 73-77.	13.7	1,771
2	Femtosecond diffractive imaging with a soft-X-ray free-electron laser. Nature Physics, 2006, 2, 839-843.	6.5	910
3	Single mimivirus particles intercepted and imaged with an X-ray laser. Nature, 2011, 470, 78-81.	13.7	790
4	High-Resolution Protein Structure Determination by Serial Femtosecond Crystallography. Science, 2012, 337, 362-364.	6.0	758
5	Crystal structure of rhodopsin bound to arrestin by femtosecond X-ray laser. Nature, 2015, 523, 561-567.	13.7	683
6	Structure of the toxic core of $\hat{I}_{\pm}$ -synuclein from invisible crystals. Nature, 2015, 525, 486-490.	13.7	528
7	Lipidic cubic phase injector facilitates membrane protein serial femtosecond crystallography. Nature Communications, 2014, 5, 3309.	5.8	505
8	Linac Coherent Light Source: The first five years. Reviews of Modern Physics, 2016, 88, .	16.4	477
9	Serial Femtosecond Crystallography of G Protein–Coupled Receptors. Science, 2013, 342, 1521-1524.	6.0	424
10	Time-resolved serial crystallography captures high-resolution intermediates of photoactive yellow protein. Science, 2014, 346, 1242-1246.	6.0	418
11	Serial time-resolved crystallography of photosystem II using a femtosecond X-ray laser. Nature, 2014, 513, 261-265.	13.7	403
12	Natively Inhibited <i>Trypanosoma brucei</i> Cathepsin B Structure Determined by Using an X-ray Laser. Science, 2013, 339, 227-230.	6.0	393
13	Structures of the intermediates of Kok's photosynthetic water oxidation clock. Nature, 2018, 563, 421-425.	13.7	386
14	Ultrafast X-ray probing of water structure below the homogeneous ice nucleation temperature. Nature, 2014, 510, 381-384.	13.7	385
15	Tracking excited-state charge and spin dynamics in iron coordination complexes. Nature, 2014, 509, 345-348.	13.7	382
16	Simultaneous Femtosecond X-ray Spectroscopy and Diffraction of Photosystem II at Room Temperature. Science, 2013, 340, 491-495.	6.0	378
17	Femtosecond structural dynamics drives the trans/cis isomerization in photoactive yellow protein. Science, 2016, 352, 725-729.	6.0	348
18	Direct observation of ultrafast collective motions in CO myoglobin upon ligand dissociation. Science, 2015, 350, 445-450.	6.0	344

#	Article	IF	CITATIONS
19	Structure of photosystem II and substrate binding at room temperature. Nature, 2016, 540, 453-457.	13.7	323
20	Structure of the Angiotensin Receptor Revealed by Serial Femtosecond Crystallography. Cell, 2015, 161, 833-844.	13.5	315
21	Structures of riboswitch RNA reaction states by mix-and-inject XFEL serial crystallography. Nature, 2017, 541, 242-246.	13.7	251
22	De novo protein crystal structure determination from X-ray free-electron laser data. Nature, 2014, 505, 244-247.	13.7	245
23	Femtosecond time-delay X-ray holography. Nature, 2007, 448, 676-679.	13.7	238
24	Single Particle X-ray Diffractive Imaging. Nano Letters, 2008, 8, 310-316.	4.5	229
25	Ultrafast single-shot diffraction imaging of nanoscale dynamics. Nature Photonics, 2008, 2, 415-419.	15.6	221
26	Taking snapshots of photosynthetic water oxidation using femtosecond X-ray diffraction and spectroscopy. Nature Communications, 2014, 5, 4371.	5.8	206
27	In vivo protein crystallization opens new routes in structural biology. Nature Methods, 2012, 9, 259-262.	9.0	193
28	Femtosecond Visualization of Lattice Dynamics in Shock-Compressed Matter. Science, 2013, 342, 220-223.	6.0	176
29	Visualizing a protein quake with time-resolved X-ray scattering at a free-electron laser. Nature Methods, 2014, 11, 923-926.	9.0	173
30	The Coherent X-ray Imaging (CXI) instrument at the Linac Coherent Light Source (LCLS). New Journal of Physics, 2010, 12, 035024.	1.2	170
31	Fixed-target protein serial microcrystallography with an x-ray free electron laser. Scientific Reports, 2014, 4, 6026.	1.6	169
32	Massively parallel X-ray holography. Nature Photonics, 2008, 2, 560-563.	15.6	168
33	Nanoflow electrospinning serial femtosecond crystallography. Acta Crystallographica Section D: Biological Crystallography, 2012, 68, 1584-1587.	2.5	167
34	The Coherent X-ray Imaging instrument at the Linac Coherent Light Source. Journal of Synchrotron Radiation, 2015, 22, 514-519.	1.0	152
35	Chromophore twisting in the excited state of a photoswitchable fluorescent protein captured by time-resolved serial femtosecond crystallography. Nature Chemistry, 2018, 10, 31-37.	6.6	152
36	Structural basis for bifunctional peptide recognition at human δ-opioid receptor. Nature Structural and Molecular Biology, 2015, 22, 265-268.	3.6	151

#	Article	IF	CITATIONS
37	Room temperature femtosecond X-ray diffraction of photosystem II microcrystals. Proceedings of the National Academy of Sciences of the United States of America, 2012, 109, 9721-9726.	3.3	144
38	Accurate macromolecular structures using minimal measurements from X-ray free-electron lasers. Nature Methods, 2014, 11, 545-548.	9.0	140
39	Femtosecond response of polyatomic molecules to ultra-intense hard X-rays. Nature, 2017, 546, 129-132.	13.7	139
40	Ultra-precise characterization of LCLS hard X-ray focusing mirrors by high resolution slope measuring deflectometry. Optics Express, 2012, 20, 4525.	1.7	132
41	A novel inert crystal delivery medium for serial femtosecond crystallography. IUCrJ, 2015, 2, 421-430.	1.0	123
42	Macromolecular diffractive imaging using imperfect crystals. Nature, 2016, 530, 202-206.	13.7	123
43	Three-dimensional view of ultrafast dynamics in photoexcited bacteriorhodopsin. Nature Communications, 2019, 10, 3177.	5.8	121
44	Liquid explosions induced by X-ray laser pulses. Nature Physics, 2016, 12, 966-971.	6.5	116
45	Energy-dispersive X-ray emission spectroscopy using an X-ray free-electron laser in a shot-by-shot mode. Proceedings of the National Academy of Sciences of the United States of America, 2012, 109, 19103-19107.	3.3	113
46	Protein crystal structure obtained at 2.9 Ã resolution from injecting bacterial cells into an X-ray free-electron laser beam. Proceedings of the National Academy of Sciences of the United States of America, 2014, 111, 12769-12774.	3.3	111
47	Indications of radiation damage in ferredoxin microcrystals using high-intensity X-FEL beams. Journal of Synchrotron Radiation, 2015, 22, 225-238.	1.0	110
48	CSPAD-140k: A versatile detector for LCLS experiments. Nuclear Instruments and Methods in Physics Research, Section A: Accelerators, Spectrometers, Detectors and Associated Equipment, 2013, 718, 550-553.	0.7	106
49	Concentric-flow electrokinetic injector enables serial crystallography of ribosome and photosystem II. Nature Methods, 2016, 13, 59-62.	9.0	103
50	Anomalous Behavior of the Homogeneous Ice Nucleation Rate in "No-Man's Land― Journal of Physical Chemistry Letters, 2015, 6, 2826-2832.	2.1	102
51	The CSPAD megapixel x-ray camera at LCLS. Proceedings of SPIE, 2012, , .	0.8	99
52	Anomalous nonlinear X-ray Compton scattering. Nature Physics, 2015, 11, 964-970.	6.5	99
53	De novo phasing with X-ray laser reveals mosquito larvicide BinAB structure. Nature, 2016, 539, 43-47.	13.7	98
54	Native phasing of x-ray free-electron laser data for a G protein–coupled receptor. Science Advances, 2016, 2, e1600292.	4.7	97

#	Article	IF	CITATIONS
55	Mechanism and dynamics of fatty acid photodecarboxylase. Science, 2021, 372, .	6.0	93
56	Double-flow focused liquid injector for efficient serial femtosecond crystallography. Scientific Reports, 2017, 7, 44628.	1.6	90
57	Toxicity of Eosinophil MBP Is Repressed by Intracellular Crystallization and Promoted by Extracellular Aggregation. Molecular Cell, 2015, 57, 1011-1021.	4.5	88
58	Femtosecond X-ray diffraction from two-dimensional protein crystals. IUCrJ, 2014, 1, 95-100.	1.0	78
59	Structure of a photosynthetic reaction centre determined by serial femtosecond crystallography. Nature Communications, 2013, 4, 2911.	5.8	74
60	Ultrafast X-ray scattering reveals vibrational coherence following Rydberg excitation. Nature Chemistry, 2019, 11, 716-721.	6.6	73
61	Protein structure determination by single-wavelength anomalous diffraction phasing of X-ray free-electron laser data. IUCrJ, 2016, 3, 180-191.	1.0	71
62	Lipidic cubic phase injector is a viable crystal delivery system for time-resolved serial crystallography. Nature Communications, 2016, 7, 12314.	5.8	71
63	Transient lattice contraction in the solid-to-plasma transition. Science Advances, 2016, 2, e1500837.	4.7	70
64	Snapshot of an oxygen intermediate in the catalytic reaction of cytochrome <i>c</i> oxidase. Proceedings of the National Academy of Sciences of the United States of America, 2019, 116, 3572-3577.	3.3	70
65	Atomic structure of granulin determined from native nanocrystalline granulovirus using an X-ray free-electron laser. Proceedings of the National Academy of Sciences of the United States of America, 2017, 114, 2247-2252.	3.3	65
66	Coherent diffraction of single Rice Dwarf virus particles using hard X-rays at the Linac Coherent Light Source. Scientific Data, 2016, 3, 160064.	2.4	64
67	Experimental strategies for imaging bioparticles with femtosecond hard X-ray pulses. IUCrJ, 2017, 4, 251-262.	1.0	63
68	Serial femtosecond crystallography of soluble proteins in lipidic cubic phase. IUCrJ, 2015, 2, 545-551.	1.0	61
69	Sacrificial Tamper Slows Down Sample Explosion in FLASH Diffraction Experiments. Physical Review Letters, 2010, 104, 064801.	2.9	59
70	Structural dynamics in proteins induced by and probed with X-ray free-electron laser pulses. Nature Communications, 2020, 11, 1814.	5.8	57
71	Performance of a beam-multiplexing diamond crystal monochromator at the Linac Coherent Light Source. Review of Scientific Instruments, 2014, 85, 063106.	0.6	55
72	High-accuracy wavefront sensing for x-ray free electron lasers. Optica, 2018, 5, 967.	4.8	53

#	Article	IF	CITATIONS
73	X-ray laser diffraction for structure determination of the rhodopsin-arrestin complex. Scientific Data, 2016, 3, 160021.	2.4	51
74	Stimulated X-Ray Emission Spectroscopy in Transition Metal Complexes. Physical Review Letters, 2018, 120, 133203.	2.9	48
75	Ultrafast structural changes within a photosynthetic reaction centre. Nature, 2021, 589, 310-314.	13.7	47
76	How Cubic Can Ice Be?. Journal of Physical Chemistry Letters, 2017, 8, 3216-3222.	2.1	46
77	Establishing nonlinearity thresholds with ultraintense X-ray pulses. Scientific Reports, 2016, 6, 33292.	1.6	43
78	Optical laser systems at the Linac Coherent Light Source. Journal of Synchrotron Radiation, 2015, 22, 526-531.	1.0	42
79	Observation of the molecular response to light upon photoexcitation. Nature Communications, 2020, 11, 2157.	5.8	42
80	Femtosecond diffractive imaging of biological cells. Journal of Physics B: Atomic, Molecular and Optical Physics, 2010, 43, 194015.	0.6	41
81	Early-stage dynamics of chloride ion–pumping rhodopsin revealed by a femtosecond X-ray laser. Proceedings of the National Academy of Sciences of the United States of America, 2021, 118, .	3.3	41
82	Aerosol Imaging with a Soft X-Ray Free Electron Laser. Aerosol Science and Technology, 2010, 44, i-vi.	1.5	40
83	Selenium single-wavelength anomalous diffraction de novo phasing using an X-ray-free electron laser. Nature Communications, 2016, 7, 13388.	5.8	40
84	Negative Pressures and Spallation in Water Drops Subjected to Nanosecond Shock Waves. Journal of Physical Chemistry Letters, 2016, 7, 2055-2062.	2.1	40
85	The room temperature crystal structure of a bacterial phytochrome determined by serial femtosecond crystallography. Scientific Reports, 2016, 6, 35279.	1.6	39
86	The Macromolecular Femtosecond Crystallography Instrument at the Linac Coherent Light Source. Journal of Synchrotron Radiation, 2019, 26, 346-357.	1.0	37
87	Determining Orientations of Optical Transition Dipole Moments Using Ultrafast X-ray Scattering. Journal of Physical Chemistry Letters, 2018, 9, 6556-6562.	2.1	36
88	A deep UV trigger for ground-state ring-opening dynamics of 1,3-cyclohexadiene. Science Advances, 2019, 5, eaax6625.	4.7	35
89	Camera for coherent diffractive imaging and holography with a soft-x-ray free-electron laser. Applied Optics, 2008, 47, 1673.	2.1	34
90	A single-shot intensity-position monitor for hard x-ray FEL sources. Proceedings of SPIE, 2011, , .	0.8	34

#	Article	IF	CITATIONS
91	Femtosecond X-ray coherent diffraction of aligned amyloid fibrils on low background graphene. Nature Communications, 2018, 9, 1836.	5.8	34
92	Serial femtosecond X-ray diffraction of 30S ribosomal subunit microcrystals in liquid suspension at ambient temperature using an X-ray free-electron laser. Acta Crystallographica Section F: Structural Biology Communications, 2013, 69, 1066-1069.	0.7	32
93	7 Ã resolution in protein two-dimensional-crystal X-ray diffraction at Linac Coherent Light Source. Philosophical Transactions of the Royal Society B: Biological Sciences, 2014, 369, 20130500.	1.8	32
94	Low-Zpolymer sample supports for fixed-target serial femtosecond X-ray crystallography. Journal of Applied Crystallography, 2015, 48, 1072-1079.	1.9	32
95	Comparing serial X-ray crystallography and microcrystal electron diffraction (MicroED) as methods for routine structure determination from small macromolecular crystals. IUCrJ, 2020, 7, 306-323.	1.0	32
96	The New Macromolecular Femtosecond Crystallography (MFX) Instrument at LCLS. Synchrotron Radiation News, 2016, 29, 23-28.	0.2	31
97	Serial femtosecond crystallography on in vivo-grown crystals drives elucidation of mosquitocidal Cyt1Aa bioactivation cascade. Nature Communications, 2020, 11, 1153.	5.8	31
98	Ternary structure reveals mechanism of a membrane diacylglycerol kinase. Nature Communications, 2015, 6, 10140.	5.8	30
99	Relativistic and resonant effects in the ionization of heavy atoms by ultra-intense hard X-rays. Nature Communications, 2018, 9, 4200.	5.8	29
100	Strongly aligned gas-phase molecules at free-electron lasers. Journal of Physics B: Atomic, Molecular and Optical Physics, 2015, 48, 204002.	0.6	28
101	Ultrafast nonthermal heating of water initiated by an X-ray Free-Electron Laser. Proceedings of the National Academy of Sciences of the United States of America, 2018, 115, 5652-5657.	3.3	28
102	Non-destructive characterization and alignment of aerodynamically focused particle beams using single particle charge detection. Journal of Aerosol Science, 2008, 39, 917-928.	1.8	26
103	Simplicity Beneath Complexity: Counting Molecular Electrons Reveals Transients and Kinetics of Photodissociation Reactions. Angewandte Chemie - International Edition, 2019, 58, 6371-6375.	7.2	25
104	Towards phasing using high X-ray intensity. IUCrJ, 2015, 2, 627-634.	1.0	24
105	X-ray diffractive imaging of controlled gas-phase molecules: Toward imaging of dynamics in the molecular frame. Journal of Chemical Physics, 2020, 152, 084307.	1.2	24
106	The ePix10k 2-megapixel hard X-ray detector at LCLS. Journal of Synchrotron Radiation, 2020, 27, 608-615.	1.0	24
107	Coherent diffractive imaging of microtubules using an X-ray laser. Nature Communications, 2019, 10, 2589.	5.8	22
108	Femtosecond quantification of void evolution during rapid material failure. Science Advances, 2020, 6, .	4.7	22

#	Article	IF	CITATIONS
109	Effect of X-ray free-electron laser-induced shockwaves on haemoglobin microcrystals delivered in a liquid jet. Nature Communications, 2021, 12, 1672.	5.8	21
110	Effects of self-seeding and crystal post-selection on the quality of Monte Carlo-integrated SFX data. Journal of Synchrotron Radiation, 2015, 22, 644-652.	1.0	20
111	Demonstration of simultaneous experiments usingÂthin crystal multiplexing at the Linac CoherentÂLight Source. Journal of Synchrotron Radiation, 2015, 22, 626-633.	1.0	20
112	X-ray laser–induced electron dynamics observed by femtosecond diffraction from nanocrystals of Buckminsterfullerene. Science Advances, 2016, 2, e1601186.	4.7	20
113	Advances in ultrafast gas-phase x-ray scattering. Journal of Physics B: Atomic, Molecular and Optical Physics, 2020, 53, 234004.	0.6	20
114	Structural studies of P-type ATPase–ligand complexes using an X-ray free-electron laser. IUCrJ, 2015, 2, 409-420.	1.0	20
115	Focal Spot and Wavefront Sensing of an X-Ray Free Electron laser using Ronchi shearing interferometry. Scientific Reports, 2017, 7, 13698.	1.6	19
116	3D printed droplet generation devices for serial femtosecond crystallography enabled by surface coating. Journal of Applied Crystallography, 2019, 52, 997-1008.	1.9	19
117	Coherent X-ray diffractive imaging of protein crystals. Journal of Synchrotron Radiation, 2008, 15, 576-583.	1.0	18
118	Ultrafast X-ray scattering offers a structural view of excited-state charge transfer. Proceedings of the United States of America, 2021, 118, .	3.3	18
119	Characterization and use of the spent beam for serial operation of LCLS. Journal of Synchrotron Radiation, 2015, 22, 634-643.	1.0	17
120	Synchronous RNA conformational changes trigger ordered phase transitions in crystals. Nature Communications, 2021, 12, 1762.	5.8	17
121	Ultrafast soft X-ray scattering and reference-enhanced diffractive imaging of weakly scattering nanoparticles. Journal of Electron Spectroscopy and Related Phenomena, 2008, 166-167, 65-73.	0.8	16
122	Scattering off molecules far from equilibrium. Journal of Chemical Physics, 2019, 151, 084301.	1.2	16
123	Analysis of XFEL serial diffraction data from individual crystalline fibrils. IUCrJ, 2017, 4, 795-811.	1.0	16
124	Experience with the CSPAD during dedicated detector runs at LCLS. Journal of Physics: Conference Series, 2014, 493, 012011.	0.3	15
125	Harnessing the power of an X-ray laser for serial crystallography of membrane proteins crystallized in lipidic cubic phase. IUCrJ, 2020, 7, 976-984.	1.0	15
126	X-ray Free Electron Laser Determination of Crystal Structures of Dark and Light States of a Reversibly Photoswitching Fluorescent Protein at Room Temperature. International Journal of Molecular Sciences, 2017, 18, 1918.	1.8	14

#	Article	IF	CITATIONS
127	Flowâ€aligned, singleâ€shot fiber diffraction using a femtosecond Xâ€ray freeâ€electron laser. Cytoskeleton, 2017, 74, 472-481.	1.0	12
128	Radiation driven collapse of protein crystals. Journal of Synchrotron Radiation, 2006, 13, 1-7.	1.0	11
129	Serial femtosecond X-ray diffraction of enveloped virus microcrystals. Structural Dynamics, 2015, 2, 041720.	0.9	11
130	Performance of ePix10K, a high dynamic range, gain auto-ranging pixel detector for FELs. AIP Conference Proceedings, 2019, , .	0.3	11
131	Generation of high-intensity ultrasound through shock propagation in liquid jets. Physical Review Fluids, 2019, 4, .	1.0	11
132	Nanocrystallography measurements of early stage synthetic malaria pigment. Journal of Applied Crystallography, 2017, 50, 1533-1540.	1.9	11
133	Serial femtosecond crystallography datasets from G protein-coupled receptors. Scientific Data, 2016, 3, 160057.	2.4	10
134	Double grating shearing interferometry for X-ray free-electron laser beams. Optica, 2020, 7, 404.	4.8	9
135	X-ray Emission Spectroscopy at X-ray Free Electron Lasers: Limits to Observation of the Classical Spectroscopic Response for Electronic Structure Analysis. Journal of Physical Chemistry Letters, 2019, 10, 441-446.	2.1	8
136	Observation of shock-induced protein crystal damage during megahertz serial femtosecond crystallography. Physical Review Research, 2021, 3, .	1.3	8
137	X-Ray Free Electron Lasers and Their Applications. , 2018, , 1-21.		8
138	Resolution extension by image summing in serial femtosecond crystallography of two-dimensional membrane-protein crystals. IUCrJ, 2018, 5, 103-117.	1.0	8
139	Lifetime and damage threshold properties of reflective x-ray coatings for the LCLS free-electron laser. Proceedings of SPIE, 2011, , .	0.8	7
140	Expression, purification and crystallization of CTB-MPR, a candidate mucosal vaccine component against HIV-1. IUCrJ, 2014, 1, 305-317.	1.0	6
141	Silicon Mirrors for High-Intensity X-Ray Pump and Probe Experiments. Physical Review Applied, 2014, 1, .	1.5	6
142	Se-SAD serial femtosecond crystallography datasets from selenobiotinyl-streptavidin. Scientific Data, 2017, 4, 170055.	2.4	6
143	Numerical simulations of the hard X-ray pulse intensity distribution at the Linac Coherent Light Source. Journal of Synchrotron Radiation, 2017, 24, 738-743.	1.0	6
144	Observations of phase changes in monoolein during high viscous injection. Journal of Synchrotron Radiation, 2022, 29, 602-614.	1.0	5

#	Article	IF	CITATIONS
145	Diffraction data of core-shell nanoparticles from an X-ray free electron laser. Scientific Data, 2017, 4, 170048.	2.4	4
146	Short-pulse Laser Induced Transient Structure Formation and Ablation Studied with Time-resolved Coherent XUV-scattering. Materials Research Society Symposia Proceedings, 2009, 1230, 1.	0.1	3
147	Measurements of Long-range Electronic Correlations During Femtosecond Diffraction Experiments Performed on Nanocrystals of Buckminsterfullerene. Journal of Visualized Experiments, 2017, , .	0.2	3
148	Development, experimental performance and damage properties of x-ray optics for the LCLS free-electron laser. , 2013, , .		2
149	A statistical approach to detect protein complexes at X-ray freeÂelectron laser facilities. Communications Physics, 2018, 1, .	2.0	2
150	Nanofocus characterization at the Coherent X-ray Imaging instrument using 2D single grating interferometry. , 2019, , .		2
151	Trace phase detection and strain characterization from serial X-ray free-electron laser crystallography of a Pr <sub>0.5</sub> Ca <sub>0.5</sub> MnO <sub>3</sub> powder. Powder Diffraction, 2015, 30, S25-S30.	0.4	1
152	Serial crystallography using automated drop dispensing. Journal of Synchrotron Radiation, 2021, 28, 1386-1392.	1.0	1
153	Structure-factor amplitude reconstruction from serial femtosecond crystallography of two-dimensional membrane-protein crystals. IUCrJ, 2019, 6, 34-45.	1.0	1
154	Anomalous Two-Photon Compton Scattering. New Journal of Physics, 0, , .	1.2	1
155	Probing homogenous ice nucleation within supercooled bulk water droplet in "no man's land" with an ultrafast X-ray laser. , 2013, , .		0
156	Silicon single crystal as back-reflector for high-intensity hard x-rays. , 2014, , .		0
157	Using Ultrafast X-ray Lasers to Image Structure & Dynamics. Microscopy and Microanalysis, 2015, 21, 1849-1850.	0.2	0